Applied Catalysis B: Environmental 180 (2016) 648–655

Contents lists available at ScienceDirect

Applied Catalysis B: Environmental

journal homepage: www.elsevier.com/locate/apcatb

Accelerated self-cleaning by Cu promoted semiconductor binary-oxides under low intensity sunlight irradiation

S. Rtimi [a], C. Pulgarin [a], R. Sanjines [b], J. Kiwi [a,*]

[a] Ecole Polytechnique Fédérale de Lausanne, EPFL-SB-ISIC-GPAO, Station 6, CH-1015 Lausanne, Switzerland
[b] Ecole Polytechnique Fédérale de Lausanne, EPFL-SB-IPMC-LPCM, CH-1015 Lausanne, Station 3, Switzerland

ARTICLE INFO

Article history:
Received 21 April 2015
Received in revised form 19 June 2015
Accepted 25 June 2015
Available online 15 July 2015

Keywords:
TiO_2–ZrO_2 binary oxides
Self-cleaning photocatalysis
Cu intra-gap states
Band-gap of various TiO_2–ZrO_2–Cu
Interfacial charge transfer mechanism (IFCT)

ABSTRACT

Uniform adhesive TiO_2–ZrO_2 films co-sputtered on polyester (PES) under low intensity sunlight irradiation discolored methylene blue (MB) within 120 min. The discoloration kinetics was seen to be accelerated by a factor four by TiO_2–ZrO_2–Cu containing ~0.01% Cu, as determined by X-ray fluorescence (XRF). TiO_2–ZrO_2–Cu also increased also accelerated by a factor the discoloration of MB compared to TiO_2/Cu(PES). MB discoloration was also monitored under visible light in the solar cavity by using a 400 nm cutoff filter. Photocatalyst surfaces were characterized by spectroscopic methods showing the film optical absorption and by X-ray photoelectron spectroscopy (XPS), the surface atomic percentage concentration up to 120 nm (~600 layers). The band-gaps of TiO_2–ZrO_2 and TiO_2–ZrO_2–Cu were estimated for films co-sputtered for different times. By Fourier transform attenuated infrared spectroscopy (ATR-FTIR), the systematic shift of the predominating $\nu_s(CH_2)$ vibration-rotational MB bands was monitored up to complete MB discoloration under low intensity solar simulated light. Evidence is presented for the $OH^{\bullet}$ generation by TiO_2–ZrO_2–Cu participating in the self-cleaning mechanism. The photo-induced interfacial charge transfer (IFCT) on the TiO_2–ZrO_2–Cu is discussed in terms of the electronic band positions of the binary oxides and Cu intra-gap states. This study presents the first evidence for a Cu-promoted composed of two binary oxide semiconductors accelerating the self-cleaning performance.

1. Introduction

Photocatalysis as a useful tool for the self-cleaning of glass, polymer thin films and textile fabric surfaces has recently been reported by Daoud [1–4], Kiwi [5–8], Hashimoto/Fujishima et al. [9,10], Bahnemann [11–13], Radetic [14] and Pakkanen [15]. TiO_2 has been chosen as the standard photocatalyst used in the field of environmental photochemistry due to its stability, effective separation of charges under band-gap irradiation and availability of fairly pure samples. The self-cleaning by TiO_2 modified surfaces its basically a photo-oxidative process requiring sunlight, O_2 (air) and water vapor (air) to produce highly oxidative radicals able to destroy organic compounds [9,10].

There is nowadays a need to develop resistant photocatalysts presenting faster self-cleaning kinetics compared to TiO_2 and composite-TiO_2 surfaces which are too slow for many industrial applications [5–8,11–13]. The second area that needs improvement lies in the fact that most of the self-cleaning films are deposited from colloids on surfaces that are subsequently heated to diffuse and anneal the colloid into the surface at temperatures that fabrics and polymer films do not resist [5–13]. The deposition/adhesion of this non-uniform low adhesive colloidal TiO_2 films are easily wiped out by finger or cloth since they are not mechanically stable. Direct current magnetron sputtering (DCMS) is used in this study to overcome the non-uniformity and low adhesion of colloidal films [16–19]. We used DCMS to sputter uniform adhesive innovative TiO_2–ZrO_2 and TiO_2–ZrO_2–Cu at temperatures <140 °C, below the polyester (PES) limit of thermal resistance. The DACRON-PES used in this study will be shown to be a suitable substrate for TiO_2–ZrO_2–Cu films decomposing with a fast kinetics organic compounds/dyes under light irradiation. As a result of the present investigation, we present a suitable film preparation and evaluation of the observed accelerated self-cleaning kinetics showing film uniformity/adhesion, two drawbacks observed TiO_2 colloidal coated surfaces [16–18].

Self-cleaning surfaces are labor and energy saving materials [11]. We address hereby innovative self-cleaning by TiO_2–ZrO_2 and TiO_2–ZrO_2–Cu films on PES reducing the self-cleaning time of methylene blue (MB). In the past our laboratory has worked on the self-cleaning of wine stains by TiO_2 on fabrics within 24 h

* Corresponding author. Tel.: 004121 69 36150. fax: +41 21 693 5690.
E-mail address: john.kiwi@epfl.ch (J. Kiwi).

http://dx.doi.org/10.1016/j.apcatb.2015.06.047
0926-3373/

[1,5–8,13]. The self-cleaning performances of the TiO_2–ZrO_2 and TiO_2–ZrO_2–Cu PES were compared with the self-cleaning performance of MB on PE-TiO_2 under Suntest light irradiation using the same experimental conditions [19].

MB was used as a probe during this self-cleaning and has been extensively reported by Kamat [20] and Devi [21]. The MB discoloration has been generally accepted as a test method to evaluate the self-cleaning performance of photocatalytic surfaces [22]. More recently, A. Mills reported work on the MB photo-induced abatement/discoloration [23,24]. The photobleaching/degradation mechanism of MB sensitized on TiO_2 suspensions/colloids in aqueous solution is still controversial. Herrmann has recently reported the degradation pathway and intermediates of MB in colloidal solutions under light [25]. These studies take advantage of the fact that TiO_2 presents dense surface TiOH groups, high crystallinity and redox properties generating highly oxidative radicals under band-gap irradiation leading to MB degradation.

Until now, TiO_2–ZrO_2 films prepared by sol–gel methods and used as powders or annealed on diverse substrates at a few hundred degrees have been used in industrial processes as catalysis, electronic devices and in optical applications [26,27]. The effect of Cu at very low concentrations related to TiO_2–ZrO_2–Cu films will be investigated for their role hindering the TiO_2 charges recombination. The role of the intra-gap Cu-states facilitating the indirect transitions from the TiO_2vb to the TiO_2cb will be suggested in this study TiO_2–ZrO_2 films have been recently reported showing photocatalytic properties, but have not been investigated as photocatalysts for self-cleaning processes [28,29].

This investigation addresses the photocatalysis of the TiO_2–ZrO_2 and TiO_2–ZrO_2–Cu films taking MB as a probe under low intensity solar simulated sunlight. This study focuses on: (a) the preparation robust adhesive films of Cu-promoted TiO_2–ZrO_2 films by direct current magnetron sputtering (DCMS), (b) the self-cleaning kinetics of MB by TiO_2–ZrO_2–Cu films under low intensity sunlight irradiation, (c) the investigation of the surface properties of the self-cleaning films (d) the photo-induced interfacial charge transfer (IFCT) between TiO_2, ZrO_2 and Cu and finally (e) the stretching vibration shift of the MB—(CH_2) groups leading to bond scission preceding MB discoloration.

2. Experimental

2.1. Co-sputtering of TiO_2–ZrO_2 and Cu on PES and X-ray fluorescence determination of the films content and determination of the film thickness by profilometry

Thin Ti and Zr films were sputtered on PES by magnetron sputtering in a reactive oxygen atmosphere using a 50%–50% mixed targets of Ti and Zr from K. Lesker, Hastings, UK. The substrate-to-target distance was 10 cm and the targets were 2 in. in diameter. Cu on TiO_2-ZrO_2 layers was subsequently sputtered for times $\leq$10 s.

The PES used was Dacron, type 54 spun, plain weave ISO 105-F04 (EMPA) used for color fatness determinations. The nominal thickness calibration of the TiO_2–ZrO_2 films was carried out on Si-wafers with a profilometer (Alphastep500, TENCOR) and the results are shown in Fig. 1. The TiO_2-ZrO_2 shown in trace (1) is seen to be less thick compared to TiO_2–ZrO_2–Cu film shown in Fig. 2. This has the important implication that after 8 min – the coating thickness showing the fastest MB discoloration – a sputtering thickness of ~96 nm (480 layers) was attained for the TiO_2–ZrO_2 film compared to ~116 nm (580 layers) for TiO_2–ZrO_2–Cu film.

The TiO_2, ZrO_2 and Cu-content in the samples were evaluated by X-ray fluorescence in a PANalytical PW 2400 unit as a function of the sputtering time.

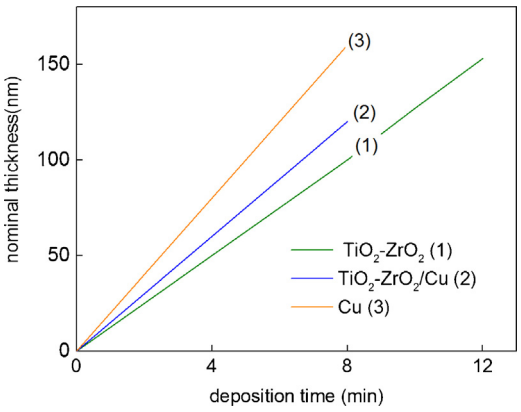

Fig. 1. Thickness calibration of TiO_2–ZrO_2 and TiO_2–ZrO_2/Cu sputtered films on Si wafers.

2.2. Diffuse reflectance spectroscopy (DRS, X-ray crystallography (XRD) and composite band-gap determination.

Diffuse reflectance spectroscopy (DRS) of the 100 μl MB stained PES samples was carried out in a PerkinElmer Lambda 900 UV–VIS-NIR spectrometer within the wavelength range of 200–800 nm. The rough UV–vis reflectance data cannot be used directly to assess the optical absorption of the samples because of the large scattering contribution of the PES fabric to the DRS spectra. Normally a weak dependence is assumed for the scattering coefficient S on the wavelength. The crystalline structures of the samples reported in this study were investigated by X-ray diffraction (XRD) by means of an INEL Model XRG instrument 3.5 KW power with a detector to register θ peaks from 2° to 120°. The spectra obtained by diffusion reflectance spectroscopy (DRS) were plotted in Kubelka–Munk (KM) units and this information was used to draw the band-gap plots for TiO_2–ZrO_2 and TiO_2–ZrO_2–Cu following the Tauc's method [30].

2.3. Irradiation procedures, visual appearance and X-ray photoelectron spectroscopy (XPS) of sputtered uniform films

The sputtered samples were irradiated with the Xe-400 W lamp in the Suntest solar simulator CPS (Atlas GmbH, Hanau, Germany) with a light dose of 50 mW/cm^2 (~0.8×10^{16} photons/s). A cut-off filter was inserted in the Suntest cavity to filter the light <310 nm. The visual perception of the discoloration of the MB-stain on PES is presented below in Fig. 4. The discoloration is visualized by the blue

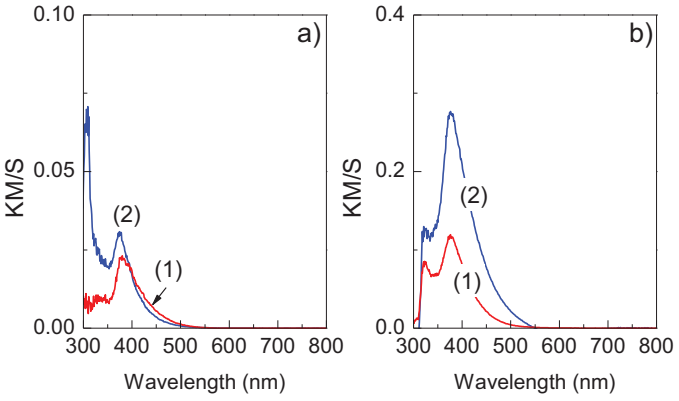

Fig. 2. (a) Diffuse Reflectance Spectroscopy (DRS) of TiO_2–ZrO_2 sputtered for (1) 8 min and (2) 12 min, (b) Diffuse Reflectance Spectroscopy (DRS) of TiO_2–ZrO_2/Cu sputtered for (1) 8 min/5s and (2) 8 min/10 s.

Table 1
XRF determination of wt% of TiO_2, ZrO_2 and Cu sputtered on polyester (PES).

	Wt% TiO_2/wt PES	Wt% ZrO_2/wt PES	Wt% Cu/wt PES
TiO_2–ZrO_2 (6 min)	0.42	0.54	
TiO_2–ZrO_2 (8 min)	0.47	0.47	
TiO_2–ZrO_2 (12 min)	0.44	0.52	
TiO_2–ZrO_2/Cu (8 min/5 s)	0.47	0.47	0.01
TiO_2–ZrO_2/Cu (8 min/10 s)	0.45	0.48	0.02

stain disappearing progressively as a function of the solar simulated Suntest irradiation time.

An AXIS NOVA photoelectron spectrometer (Kratos Analytical, Manchester, UK) equipped with monochromatic AlKα ($h\nu$ = 1486.6 eV) anode was used during the study. The carbon C1s position at 284.6 eV was the reference to reference the peak positions of C, O, Ti, Zr and Cu in the XPS spectrogram [31,32]. The Shirley correction was used to correct the electrostatic charging effect during the XPS measurement [33]. The XPS spectra were deconvoluted by means of the software CasaXPS-Vision 2 (Kratos Analytical, UK).

2.4. Monitoring oxidative radicals on TiO_2–ZrO_2–Cu fluorescence

The detection of the oxidative species (mainly $OH^{\bullet}$) was carried out according to Hashimoto [39]. Terephthalic acid 99% was an Across Chem Ltd. Product and the NaOH 98% was from Sigma–Aldrich. A sample of 4 cm^2 of TiO_2–ZrO_2–Cu coated fabric was immersed in a solution made of terephthalic acid at 0.4 mM dissolved in a 4 mM NaOH solution. After each irradiation, the solution was transferred in a quartz cell and the fluorescence spectra of 2-hydroxyterephthalic acid generated by the reaction of terephthalic acid with the OH containing compound were measured on a PerkinElmer LS-50B fluorescence spectrometer. The spectra were recorded between 400 and 500 nm (scan rate: 100 nm/min) under an excitation at 315 nm.

2.5. Infrared spectroscopy (ATR-FTIR) and light irradiation source

FTIR spectra were measured in a Portmann Instruments AG spectrophotometer equipped with a Specac attachment (45° one pass diamond crystal). Spectra were taken by 256 scans with a resolution of 2 cm^{-1} in the range 900–4000 cm^{-1}. The position of the IR peaks was found by the second derivative of the spectra after Fourier deconvolution.

3. Results and discussion

3.1. Coating content determined by X-ray fluorescence (XRF) and sample diffuse reflectance spectroscopy of the samples (DRS).

The TiO_2–ZrO_2–Cu films co-sputtered for 8 min were subsequently Cu-sputtered for 5 s and 10 s and attained the content of: 0.47% TiO_2 and 0.47% ZrO_2 weight/weight PES and 0.01% as shown in Table 1. To further characterize the optical properties of the later film the DRS spectra of sputtered samples for 8 min is presented in Fig. 2 in Kubelka–Munk units. The rough UV–vis reflectance cannot be used directly to assess the absorption coefficient of the PE-TiO_2.

Fig. 2(a) presents the TiO_2–ZrO_2 DRS spectra sputtered for two different times. The indirect electron transition of the vb electron under light occurring from the valence TiO_2 O_2p band to the Ti_3d conduction band is shown rising up at to 380 nm. The optical absorption below 380 nm in Fig. 2 is due to the ZrO_2 optical absorption with band gap ~4.5 depending on particle size [10,13].

Fig. 2(b) presents the DRS spectroscopy of TiO_2–ZrO_2–Cu sputtered also for two different times being very similar to the

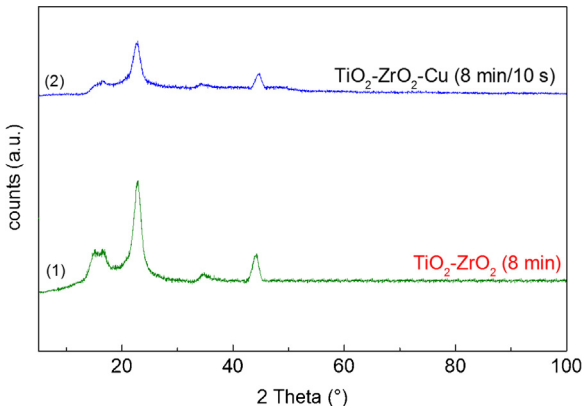

Fig. 3. XRD spectrogram of TiO_2–ZrO_2 and TiO_2–ZrO_2/Cu (on polyester (PES)).

TiO_2–ZrO_2 spectra. The amount of Cu sputtered on PES is very small as shown in Table 1, possibly developing Cu-plasmon bands too small to be registered in the visible region >500 nm (Fig. 2b). Cu has been reported to modify the energy range of TiO_2–ZrO_2 involving Cu(II) and (Cu(I) reduction to Cu° at potentials of 0.15 eV and 0.34 eV. [43,35]. By DRS (Fig. 2), XRD (Fig. 3) and by XPS (Fig. 5b) we did not find an unambiguous evidence proof for the presence of CuO, Cu_2O or Cu particles at the very low concentration of 0.02% by weight on TiO_2–ZrO_2. Recently Cu(II) in an amorphous CuO structure grafted on TiO_2 was reported to present a five coordinated square pyramidal form on TiO_2 surfaces effective in 2-propanol photocatalytic oxidation [36,37]. Cu(II) oxide-Fe(III) nanoclusters were also reported for photocatalytic oxidation of 2-propanol [38].

How the Cu-enters when decorating the TiO_2 or TiO_2–ZrO_2, interstitially or substitutionally? This remains an open question as reported recently Choi [36]. Cu does not exist as a separate layer as no distinct bands of Cu are detected in Fig. 1 consistent with recent reports [26,35,37–39].

Electron transfer from ZrO_2 to TiO_2 has been reported to drive the formation of the Ti–O–Zr-bonds [35–36]. Fig. 2a and b shows a broad spectral shoulder spectral region between 320 and 340 nm. The shoulder in the spectral region in Fig. 2a, have been reported due to interparticle Zr–O–Ti bridges between the TiO_2 and ZrO_2 oxides [36]. The XRD peaks presented in Fig. 3 for TiO_2 correspond to anatase in the TiO_2–ZrO_2 and TiO_2–ZrO_2–Cu XRD spectrogram. The anatase form is expected since the samples have been sputtered at temperatures (<140 °C).

In the double-oxide film, the Zr^{4+}-ion (r = 0.86 Å) replaces the Ti^{4+}-ion (r = 0.74 Å) ions precluding the formation of TiO_2 domains. This is due to the molecular mixing of the TiO_2 and ZrO_2 in the crystallographic network. Fig. 2 shows the TiO_2/ZrO_2 composites

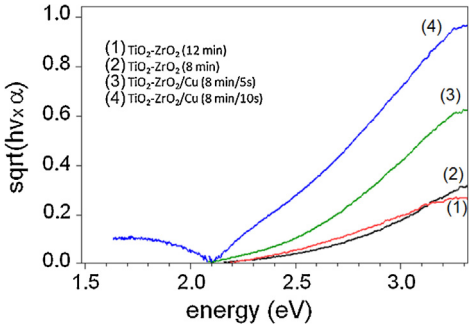

Fig. 4. Tauc's plot spectra showing the indirect transition on: (1) TiO_2–ZrO_2 sputtered on PES for 8 min followed by Cu(10 s), (2) TiO_2–ZrO_2 sputtered on PES for 8 min followed by Cu(5 s), (3) TiO_2–ZrO_2 sputtered on PES for 12 min, (4) TiO_2–ZrO_2 sputtered on PES for 8 min.

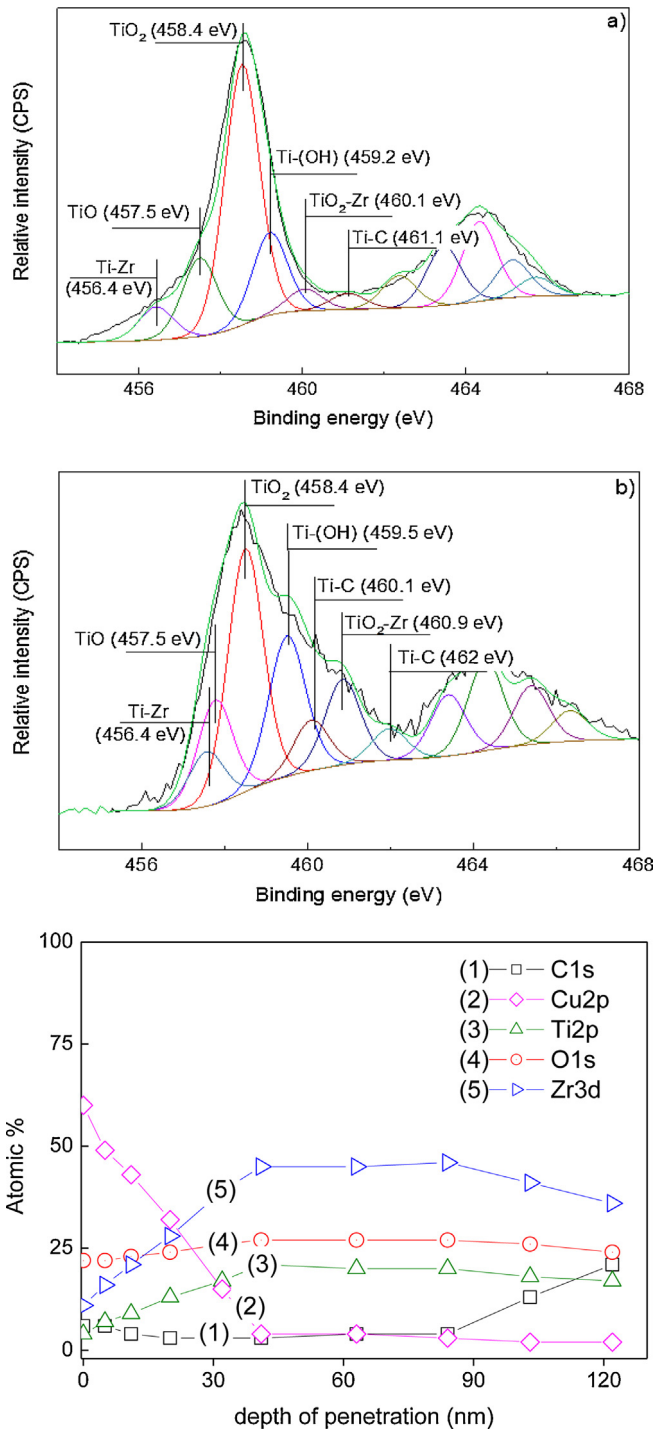

Fig. 5. (a) Deconvoluted XPS envelope of the Ti2p for TiO_2–ZrO_2/Cu PES sample sputtered for 8 min/10s before MB discoloration (time zero min). (b) Deconvoluted XPS envelope of the Ti2p for TiO_2–ZrO_2/Cu PES sample sputtered for 8 min/10 s after MB discoloration (time 30 min). (c) Percentage top-most layers atomic concentration on a sample TiO_2–ZrO_2/Cu sputtered for 8 min/10 s XPS etched by a beam of 5 kV Ar-ion showing atomic percentage as a function of penetration depth.

absorbing a larger amount of visible light compared to each oxide component taken separately. This is due to the formation of a network composed of 42% TiO_2/58% ZrO_2 (See Table 1). In agreement with the results reported by Kambur et al. [28], the DRS spectra of TiO_2 was two times higher compared to the ZrO_2, but followed a similar pattern. Surface states of ZrO_2 and TiO_2 have been reported showing TiO_2 surface trap states of ZrO_2 lying below the cb edge of TiO_2. This determines the direction of the electron flow under light irradiation [29,34,35].

Table 2
Band gap estimation of TiO_2–ZrO_2 sputtered on PES and followed by Cu deposition.

Sample	Estimated Band gap eV
TiO_2–ZrO_2 (12 min)	2.60
TiO_2–ZrO_2 (8 min)	2.47
TiO_2–ZrO_2/Cu (8 min/5 s)	2.42
TiO_2–ZrO_2/Cu (8 min/10 s)	2.25

In the hybrid TiO_2/ZrO_2 films indirect evidence of molecular mixing of TiO_2 and ZrO_2 network leading to a rise in the visible light absorption has been reported [29]. But the reasons for the increase in the light absorption has been rationalized by different groups and explained in terms of: (a) the formation of intermediate energy levels, (b) surface trap states, (c) a modified crystallinity, (d) higher acidity, (e) increase structural defects, like lattice vacancies and (f) higher number of hydroxyl surface groups [26–29,35]. The origin of the absorption bands in TiO_2/ZrO_2 remains until now a controversial matter.

3.2. X-ray diffraction (XRD) and band-gap determination of TiO_2–ZrO_2 and TiO_2–ZrO_2–Cu

Fig. 3 presents in trace (1) the XRD of TiO_2–ZrO_2 and in trace (2) for TiO_2–ZrO_2–Cu. A decrease for the TiO_2 anatase peak and also for the ZrO_2 peak due is observed to the addition of Cu 0.02%wt Cu/wt PES. The lack of a XRD signal for Cu is due to its very low atomic percentage concentration sputtered on the double-oxide network. The Cu addition to the TiO_2–ZrO_2 double oxide film has been investigated and reported already preventing the anatase to rutile transition [26–28]. The anatase phase is present in the TiO_2–ZrO_2 double oxide film co-sputtered at 120–130 °C [9,10]. Cu does not present any absorption band in the DRS spectrum as shown Fig. 2 and does not show any additional peak in the XRD spectrogram in Fig. 3.

The DRS spectra in Fig. 2 were transformed in Kubelka Munk units *vs* the spectral energy (eV) and used next to estimate the band-gaps in Fig. 4. The Tauc's plot of sqrt($h\nu \times \alpha$) against the energy axis is shown in Fig. 4. The optical band-gap was estimated by extrapolating the linear part of the spectra *vs* the energy axis [30]. The band-gap levels in Fig. 4 refer to trace (1) TiO_2–ZrO_2–Cu (8 min/10 s) 2.26 eV, trace (2) TiO_2–ZrO_2–Cu (8 min/5 s) 2.44 eV, trace (3) TiO_2–ZrO_2 12 min, 2.59 eV, and trace (4) TiO_2–ZrO_2 8 min, 2.38 eV. Traces 3 and 4 show that band gaps change with the amount of sputtered Ti and Zr. The band gaps estimated for TiO_2–ZrO_2 shown in Table 2 are narrower than the values for the TiO_2 and ZrO_2 semiconductors of 3.2 eV and 4.5 eV, respectively [9,13]. Furthermore, Table 2 also shows that only a marginal modification is introduced on the TiO_2–ZrO_2 band gap by Cu—due to the low laying intra-gap states. This will be discussed further in Section 3.7 below.

3.3. Sample X-ray photoelectron spectroscopy (XPS)

Fig. 5c presents the atomic% composition found for the elements found in the TiO_2–ZrO_2/Cu topmost layers sputtered for 8 min/10 s. The atomic percentage of Zr, O, Ti, Cu, and C is shown as a function of the etching depth. The etching of the film surface was carried out by Ar-ions of 5 kV. The penetration on the PES surface was referenced with the known rate for Ta of 15 atomic layer/min or 3 Å/min [31]. The stable C-content is shown up to 120 nm (or 600 atomic layers) concomitant with increase in the Zr, trace (5) and the concomitant decrease of Cu within the initial 40 nm. The C-percentage in Fig. 5c, trace (1) is seen to increase beyond 90 nm concomitantly

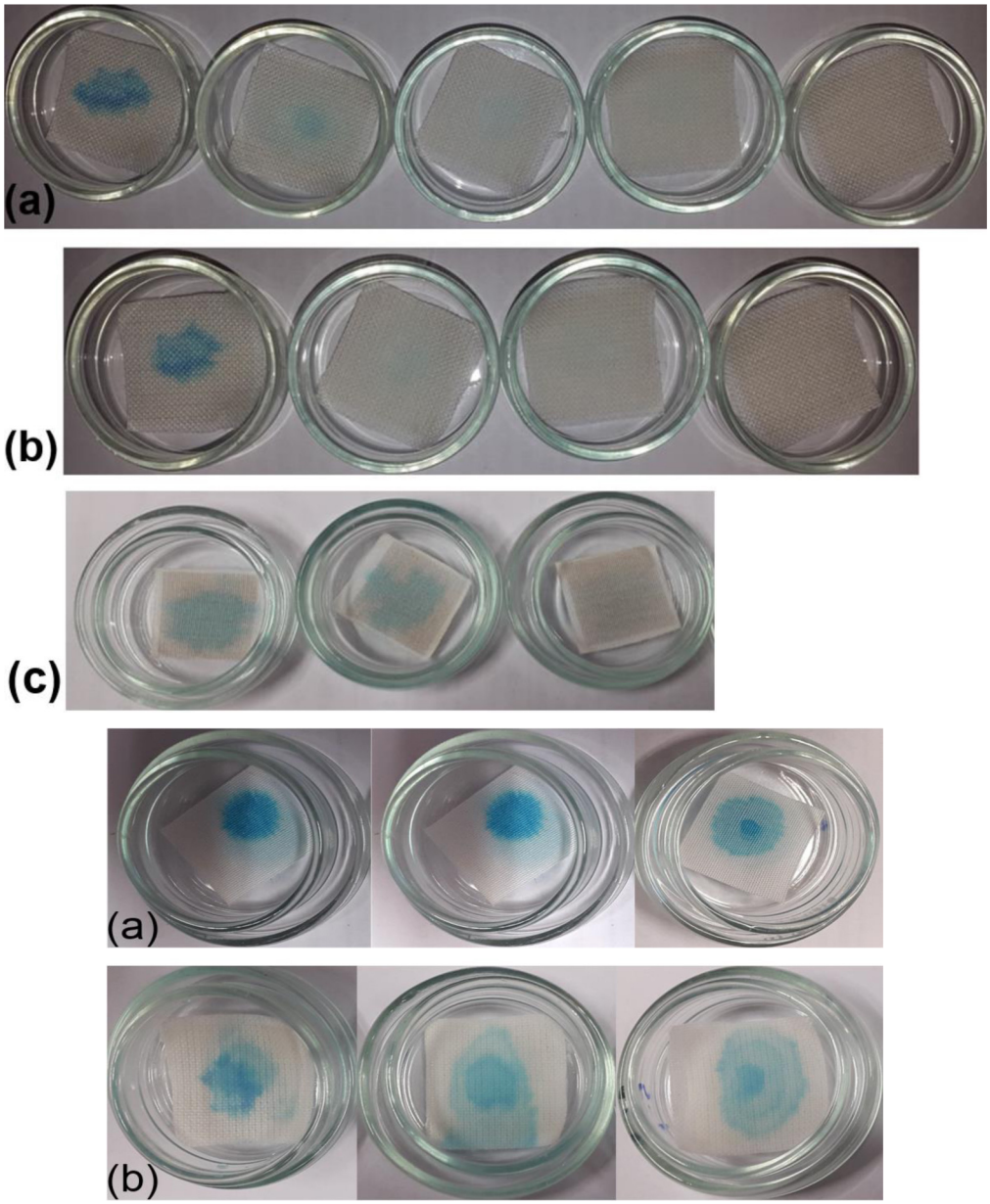

Fig. 6. (a) MB self-cleaning under irradiation under low intensity solar simulated solar Suntest light (50 mW/cm^2) on: (a) TiO_2–ZrO_2 sputtered samples for 8 min after irradiation times: 0 min; 5 min; 30 min; 60 min and 120 min, (b) TiO_2–ZrO_2/Cu sputtered for 8 min/10 s at times 0 min; 10 min; 20 min and 30 min and (c) TiO_2/Cu sputtered for 8 min/10 s at times 0 min; 30 min; and 120 min. (b) MB self-cleaning under low intensity visible light (filter cutoff 400 nm) from a solar simulated light (50 mW/cm^2) on (a) TiO_2–ZrO_2 sputtered samples for 8 min at times: 0 min; 45 min and 150 min and (b) TiO_2–ZrO_2/Cu sputtered for 8 min/10 s at times: zero min; 45 min and 150 min.

with the decrease in the Zr-content shown by trace < (5) in later discoloration stages. Ti, O and Cu are seen to remain rather constant up to 120 nm.

The shifts in binding energy (BE) of TiO_2 and ZrO_2 respect to their standard assigned levels [31–33] confirm the molecular level mixing in the composite TiO_2–ZrO_2 network active in the photocatalysis as previously reported [36,37]. Deconvoluted peaks for the Ti2p3/2 XPS envelope at time zero shows two distinct peaks with binding energies (BE) at 458.4 eV and 457.5 eV for Ti-oxides in Fig. 5a. The signal for the BE of Ti–Zr was found at 460.1 eV and 456.4 eV. Evidence for the PES substrate binding to TiO_2 is shown by the Ti–C signal at 461.1 eV. The BE band energies in eV were assigned according to references [31,32] and corrected for the electrostatic charging according to Shirley [33]. The Ti and Zr XPS-peaks did change upon Cu-sputtering and this is indicative for the integrity of the TiO_2–ZrO_2 network microstructure.

Deconvoluted peaks for the Ti2p3/2 XPS envelope after 30 min sunlight irradiation inducing MB discoloration is shown in Fig. 5b. The BE of the Ti-oxides are similar with the values found at zero time at 458.4 eV and 457.5 eV. But the BE TiO_2–Zr at 460.9 eV, Ti–C at 462.0 eV and for TiOH 459.4 eV are shifted with respect to the BE at time zero. Redox reactions take place during the MB discoloration since the shifts are > 0.2 eV [32]. Evidence for the PES substrate binding to TiO_2 before and after discoloration is shown by the Ti–C signals in both cases.

3.4. Discoloration of MB on TiO_2–ZrO_2 and TiO_2–ZrO_2–Cu under light and mechanistic considerations

Fig. 6a shows the MB self-cleaning kinetics of TiO_2–ZrO_2, TiO_2–ZrO_2–Cu and Cu/TiO_2 samples. Fig. 6a shows the MB self-cleaning induced under light on TiO_2–ZrO_2 samples occurring

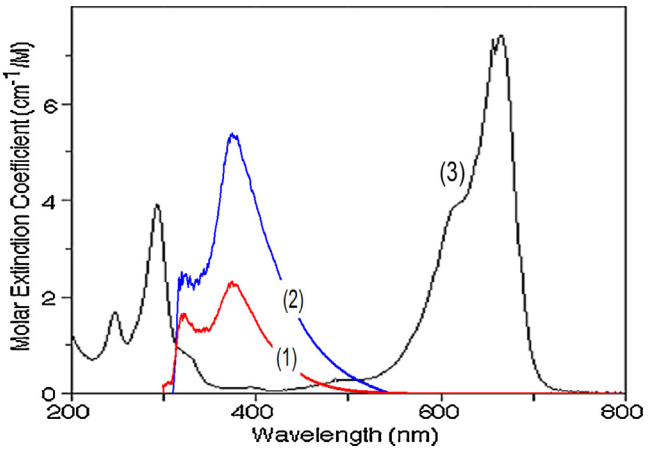

Fig. 7. Diffuse reflectance spectroscopy (DRS) of (1) TiO_2–ZrO_2/Cu sputtered for 8 min/5s, (2) 8 min/10 s and (3) methylene blue (MB).

within 120 min. This process was significantly shortened on TiO_2–ZrO_2–Cu samples (see row b) occurring within 30 min, four times faster compared to TiO_2-ZrO_2 films. TiO_2/Cu in Fig. 6a (row c) self-cleaned MB within ~120 min. This suggest a significant effect of the TiO_2–ZrO_2 matrix by the decorated of Cu affecting the kinetics of MB-discoloration.

Fig. 6b the MB self-cleaning kinetics of TiO_2–ZrO_2, TiO_2–ZrO_2–Cu under sunlight irradiation under the same experimental conditions used in Fig. 6a, but this time using a cutoff filter to block the light below 400 nm. In the case of TiO_2-ZrO_2 almost no discoloration was observed up to 150 min (row a) and when using TiO_2-ZrO_2-Cu a small MB discoloration was only forthcoming (row b).

Fig. 7 shows Ms the spectra of TiO_2–ZrO_2–Cu sputtered at two different times and also of the MB-dye. The photocatalytic discoloration of MB under solar light irradiation on TiO_2/PE has been recently reported in detail [19]. The sunlight reaching the TiO_2–ZrO_2 and TiO_2–ZrO_2–Cu uses the higher energetic photons between 350 and 500 nm available in the cavity of the Suntest simulator since it matches the spectral region of TiO_2–ZrO_2 and TiO_2–ZrO_2–Cu.

Next we discuss the reactions between the TiO_2–ZrO_2 PES under sunlight irradiation involving charge transfer reactions between MB* to ZrO_2–TiO_2.

$$MB + [TiO_2 - ZrO_2 PES] + h\nu \rightarrow [MB* \ldots TiO_2 - ZrO_2]PES \rightarrow MB^{\bullet +} + [TiO_2 - ZrO_2]PES + cbe^- \quad (1)$$

Because of the low energy absorption edge of MB at 720 nm or 1.75 eV, the electron transfer from the excited state of MB to TiO_2 is thermodynamically favored as recently reported [18]. Cu accelerating MB discoloration involves different factors such as: (a) an acceleration of the electron transfer from the valence band to the TiO_2 conduction band by Cu-intra-gap states and (b) the ZrO_2cb transfer to the TiO_2cb preventing radiative electron-hole recombination in TiO_2 [10,13] and (c) the presence of Cu/CuO surface species mediating a faster TiO_2cb to the adsorbed O_2 as shown in Eqs. (3) and (4). The participation of HO_2°/O_2^-, $OH^{\bullet}$ and h^+ species in the MB discoloration process is suggested below.

$$TiO_2 - ZrO_2 - Cu + h\nu \rightarrow h^+ + e^- \quad (2)$$

$$e^- + O_2 + H^+ \rightarrow HO_2^{\circ} E_0 - 0.05 NHE [9] \quad (3)$$

$$e^- + O_2 ads \rightarrow O_2^- ads E_0 - 0.16 NHE [10] \quad (4)$$

$$h^+ + OH^- ads \rightarrow OH^{\bullet} E_0 - 1.90 NHE [40] \quad (5)$$

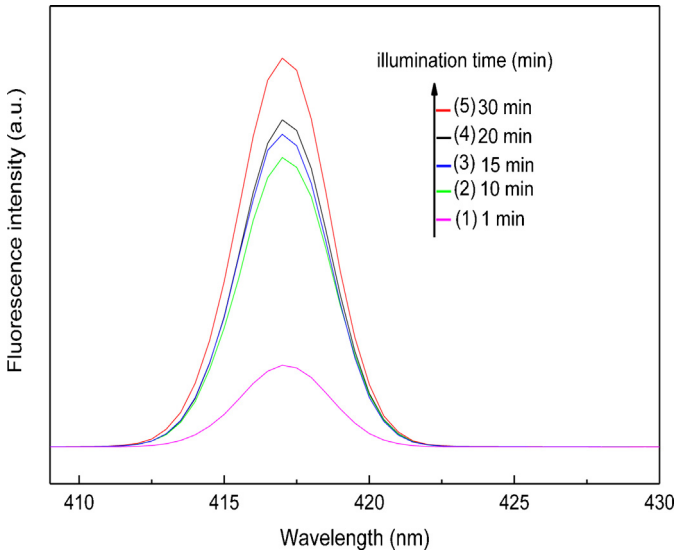

Fig. 8. $OH^{\bullet}$ production on TiO_2-ZrO_2/Cu (8 min/10 s): (1) after 1 min, (2) after 10 min, (3) after 15 min and (4) after 20 min and (5) after 30 min irradiation under low intensity solar simulated Suntest light (50 mW/cm^2).

$$h^+ + H_2 Oads \rightarrow OHads + H^+ \quad (6)$$

Doping low levels of Cu to TiO_2–ZrO_2 increased the MB discoloration rate. This may be attributed to the electron trapping at the TiO_2–ZrO_2 surface.

$$Cu^{n+} + e^- \rightarrow Cu^{(n-1)+} \quad (7)$$

Eq. (7) prevents electron-hole recombination in Eq. (2) and lead to an increased radical formation as noted in Eqs. (3)–(5). A higher Cu-doping level which is not our case, see Table 1, would allow the OH-mediated oxidation of $Cu^{(n-1)+}$ or accelerate the reverse Reaction (7). The oxidation of the reduced Cu-species in Eq. (8) would compete for the holes leading to oxidative radical species as noted in Eqs. (5)–(6)

$$Cu^{(n-1)+} + h^+ \rightarrow Cu^{n+} \quad (8)$$

Reactions (3) and (4) are thermodynamically allowed since the potential of Cu is more positive with respect to the potential required to generate electron Eqs. (3) and (4) and is more negative than the potential required for hole generation in Reaction (8).

3.5. Quantitative determination of $OH^{\bullet}$ generated within the time of MB discoloration

The enhancement of the photocatalytic efficiency by TiO_2–ZrO_2 over both TiO_2 and ZrO_2 taken independently has been reported to be due to the enhanced generation of $OH^{\bullet}$ under light irradiation [34,35]. Fig. 8 presents the evidence for the $OH^{\bullet}$ generated by TiO_2–ZrO_2–Cu under low intensity sunlight as a function of irradiation time. The increase in the fluorescence intensity is a measure of the $OH^{\bullet}$-surface generated by TiO_2–ZrO_2–Cu in solution [39] and increases with irradiation time.

3.6. FTIR-ATR spectroscopy changes within the period of MB discoloration

FTIR spectroscopy was used to monitor the MB degradation under solar simulated light. Fig. 9a presents the symmetric stretching vibration peak displacement methylene (CH_2)—IR-spectroscopy of TiO_2–ZrO_2 samples in the range 2650–2900 cm^{-1}. The IR-signals were sensitive enough to follow the IR-spectral shifts and the reduction of amplitude during MB discoloration. Fig. 9a

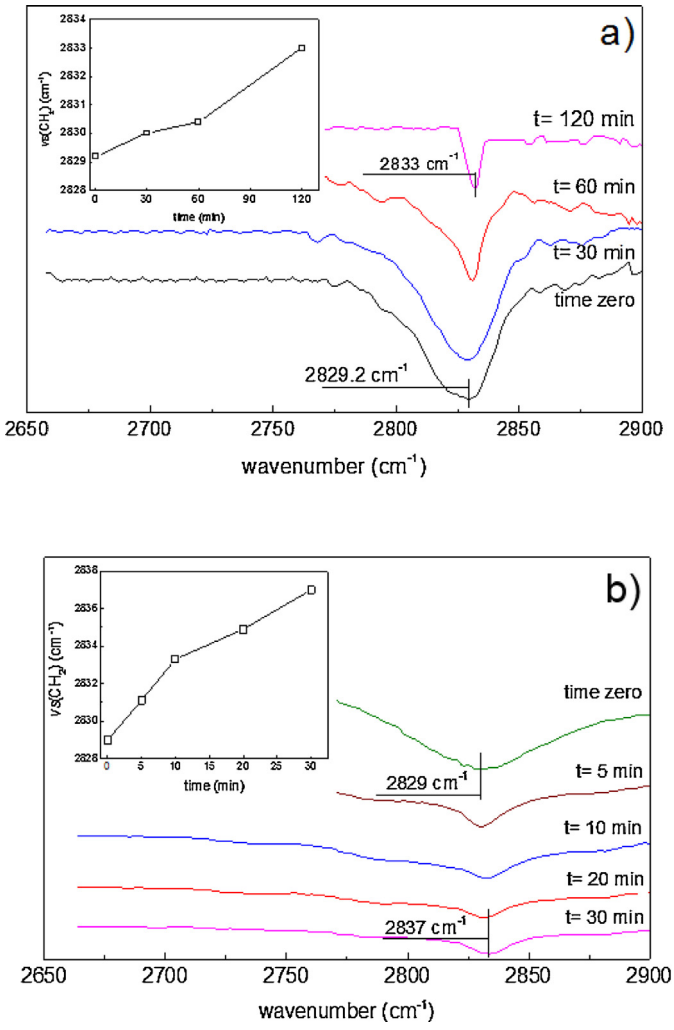

Fig. 9. (a) Shift in the MB *vs* (-CH_2) vibrational peaks in contact with TiO_2–ZrO_2 (8 min) as function of the time of irradiation, (b) Shift in the MB *vs* (—CH_2) vibrational peaks in contact with TiO_2–ZrO_2/Cu (8 min/10 s) as function of the time of irradiation in the solar simulated Suntest cavity (50 mW/cm^2).

shows a discontinuous MB IR-peak shift for methylene υ_s(—CH_2) from 2829 cm^{-1} at time zero up to 2833 cm^{-1} within 120 min, the time required for complete discoloration. Fig. 6b presents the corresponding IR-shifts mediated by a TiO_2–ZrO_2–Cu showing a similar trend during an accelerated MB-discoloration process (30 min).

The basis of this IR treatment of the data has been already reported, and therefore will not be addressed in detail in the present study [41–43]. The insert in Fig. 9a shows for a TiO_2–ZrO_2 sample a slower bond stretching of MB υ_s(—CH_2) shift up to 60 min and is followed by a steeper increase in the IR-stretching peaks after 60 min. An opposite trend is observed for the MB υ_s(—CH_2) shifts stretching bonds on TiO_2–ZrO_2–Cu. The shifts up to 10 min increase steeper compared to the increase observed at times >10 min.

3.7. *Suggested interfacial charge transfer mechanism in TiO_2–ZrO_2–Cu during MB discoloration*

The mechanism suggested in Fig. 10 is based on positions of the electronic bands of TiO_2–ZrO_2–Cu to assign the possible light induced interfacial charge transfer mechanism (IFCT). The low laying Cu intra-gap states promote the TiO_2vb (h^+) indirect transition to the TiO_2cb increasing the charge separation and decreasing the electron-hole recombination rate consistent with the results prepared in Fig. 6a and b. Cu seems to accelerate the MB self-cleaning

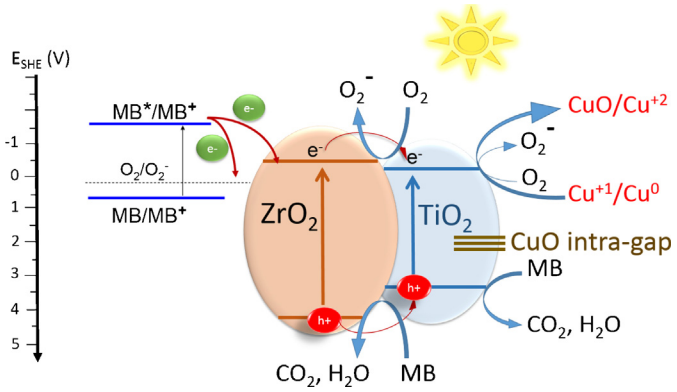

Fig. 10. Suggested scheme for the interfacial charge transfer in samples TiO_2–ZrO_2–Cu (8 min/10 s) induced by low intensity solar light (50 mW/cm^2) leading to MB discoloration/degradation. For further details see text.

kinetics. Fig. 10 presents the MB excited state (MB*) leading to short lived unstable MB*. This MB* state injects an electron into the ZrO_2cb due to the high potential of the reaction MB* → $MB^+ + e^-$ of 1.74 V NHE [18].

Cu in Fig. 10, would act acts as a trap for the TiO_2 charge carriers and not as charge recombination center due to the low Cu levels present (Table 1). The intra-gap Cu states have been suggested to accelerate the electronic transition from the conduction band to the valence band [13]. The $Cu^{1+/2+}$ deposited on TiO_2–ZrO_2 works as electron acceptor and enhance MB removal. The conduction band of CuO at −0.30 V *vs* SCE (pH 7) lies at a more negative potential than the one electron oxygen reduction potential $O_2 + H^+ + e^- \rightarrow HO_2^\circ$ −0.05 V [40] and also the oxygen reduction $e^- + O_2 \rightarrow O_2^-$ (−0.16 V). Cu^+ may also reduce O_2 consuming electrons or be oxidized to Cu-ions by the photo-generated TiO_2 holes to Cu^{2+} [9].

4. Conclusions

- Cu as a promoter in very low amounts added to the TiO_2–ZrO_2 matrix topmost layers on PES is shown to accelerate the MB-discoloration kinetics compared to TiO_2–ZrO_2 matrix alone.
- The peak shift and stretching of the symmetric MB (CH_2)-vibrations within the 30 min self-cleaning period was followed by infrared spectroscopy since the (CH_2)-groups make up >60% of the MB structure. The different shifts during the self-cleaning period for the stretching (CH_2)-vibrations observed for the TiO_2–ZrO_2 and Cu-promoted binary oxides was surprising since it occurred at Cu levels 0.01–0.02%.
- The optical band-gap of TiO_2–ZrO_2–Cu were determined to be smaller compared to TiO_2 in the interparticle network comprising Zr–O–Ti bridging.
- An IFCT mechanism is suggested to account for MB self-cleaning. The MB self-cleaning by the TiO_2 (the main sunlight absorber) is discussed considering the MB and the TiO_2–ZrO_2–Cu electronic band positions. Proof is presented for the generation of the OH• by TiO_2–ZrO_2–Cu under light.

Acknowledgments

We thank the EPFL and the EC7th Limpid FP project (Grant No 3101177) for financial support and the COST Action 1106 for interactive discussions during the course of this work.

References

[1] J. Kiwi, C. Pulgarin, Self-cleaning Materials and Surfaces, in: Walid Daoud (Ed.), Woodhead Pub. Co., UK, 2013, pp. 205–224, ch 7.

[2] S. Afzai, W. Daoud, S. Langford, ACS Appl. Mater. Interface 11 (2013) 4753–4759.
[3] W. Tung, W. Daoud, J. Mater. Chem. 21 (2011) 7858–7869.
[4] M. Lazar, W. Daoud, RSC Adv. 3 (2013) 4140–4150.
[5] A. Bozzi, T. Yuranova, J. Kiwi, J. Photochem. Photobiol. A 172 (2005) 27–34.
[6] T. Bozzi, I. Yuranova, D. Laub, J. Kiwi, J. Photochem. Photobiol. A 174 (2005) 156–164.
[7] M.I. Mejia, J.M. Marin, G. Restrepo, C. Pulgarin, E. Mielczarski, J. Mielczarski, Y. Arroyo, J.-C. Lavanchy, J. Kiwi, Appl. Catal. B 91 (2009) 481–488.
[8] M.I. Mejia, J.M. Marin, G. Restrepo, C. Pulgarin, E. Mielczarski, J. Mielczarski, J. Kiwi, ACS Appl. Mater. Interface 1 (2009) 2190–2198.
[9] X. Qiu, M. Miyaguchi, K. Sunada, M. Minoshima, M. Liu, Y. Lu, D. Li, Y. Shimodaira, Y. Hosogi, Y. Kuroda, K. Hashimoto, ACS Nano 6 (2012) 1609–1618.
[10] A. Fujishima, X. Zhang, A. Tryk, A. Donald, Surf. Sci. Rep. 63 (2008) 515–582.
[11] L. Zhang, R. Dillert, D. Bahnemann, M. Vormoor, Energy Environ. Sci. 5 (2012) 7491–7507.
[12] A.-O.L. Patrocinio, R. Paula, J. Paniago, D. Freitag Bahnemann, ACS Appl. Mater. Interface 6 (2014) 16859–16866.
[13] J. Schneider, M. Matsuoka, M. Takeuchi, J. Zhang, Y. Horiuchi, M. Anpo, D. Bahnemann, Chem. Rev. 114 (2014) 9919–9986.
[14] D. Mihailovic, Z. Saponjic, M. Radoicic, S. Lazovic, C.J. Baily, P. Jovancic, J. Nedeljkovic, M. Radetic, Cellulose 18 (2012) 811–825.
[15] J. Kasanen, M. Suvanto, T.T. Pakkanen, J. Appl. Polym. Sci. 111 (2009) 2597–2602.
[16] K. Sarakinos, J. Alami, D. Konstantinidis, Surf. Coat. Technol. 204 (2010) 1661–1684.
[17] P.J. Kelly, R.D. Arnell, Vacuum 56 (2000) 159–172.
[18] S. Rtimi, R. Sanjines, C. Pulgarin, A. Kulik, J. Kiwi, Surf. Coat. Technol. 254 (2014) 333–343.
[19] S. Rtimi, C. Pulgarin, R. Sanjines, J. Kiwi, Appl. Catal. B 162 (2015) 236–244.
[20] P.V. Kamat, Chem. Rev. 93 (2011) 267–300.
[21] S. Kumar, L. Devi, J. Phys. Chem. A 115 (2011) 13211–13241.
[22] ISO Standard 10678: 2010. Determination of the photocatalytic activity of surfaces in aqueous medium.
[23] A. Mills, Appl. Catal. B 128 (2012) 144–149.
[24] A. Mills, D. Hazafy, J. Parkinson, T. Tuttle, M. Hitchings, Dyes Pigm. 88 (2011) 149–155.
[25] A. Housas, H. Lachheb, M. Ksibi, E. Elalui, C. Guillard, J.-M. Herrmann, Appl. Catal. B 31 (2001) 145–157.
[26] X. Fu, L. Clark, Q. Yang, M. Anderson, Environ. Sci. Technol. 30 (1996) 647–653.
[27] M. Zorn, D. Tompkins, W. Zeltner, M. Anderson, Appl. Catal. B 23 (1999) 1–8.
[28] A. Kambur, G. Pozan, I. Boz, Appl. Catal. B 115-116 (2012) 149–158.
[29] Ch. Kim, H. Jeong, Bull. Korean Chem. Soc. 28 (2007) 2333–2336.
[30] J. Tauc, A. Menth, J. Non-cryst. Solids 8–10 (1972) 569.
[31] C.D. Wagner, E.L. Davis, in: G.E. Müllenberg (Ed.), Handbook of X-Ray Photoelectron Spectroscopy, Perkin-Elmer Corporation Physical Electronics Division, Minnesota, USA, 1979.
[32] J. Nogier, M. Delamar, P. Ruiz, P. Albers, J. Kiwi, Catal. Today 20 (1994) 109–123.
[33] D.A. Shirley, Phys. Rev. B 5 (1972) 4709–4714.
[34] J. Yu, J. Lin, R. Kwok, J. Phys. Chem B 102 (1998) 5094–5098.
[35] L. Tomar, B. Chakrabarty, Adv. Matter Letts. 4 (2013) 64–67.
[36] B. Neppolian, Q. Wang, H. Yamashita, H. Choi, Appl. Catal. A Gen. 333 (2007) 264–271.
[37] H. Irie, K. Kamiya, T. Shibanuma, S. Miura, D. Tryk, T. Yokoyama, K. Hashimoto, J. Phys. Chem. C 113 (2009) 10762–10766.
[38] M. Liu, X. Qiu, M. Miyauchi, K. Hashimoto, Chem. Mater. 23 (2011) 5282–5286.
[39] M. Liu, R. Inde, M. Nishikawa, X. Qiu, D. Atarashi, E. Sakai, Y. Nosaka, K. Hashimoto, M. Miyauchi, ACS Nano 8 (2014) 7229–7238.
[40] P. Wardman, J. Phys. Chem. Ref. Data 18 (1989) 1637–1755.
[41] G. Starukh, S. Toscani, S. Boursicot, L. Spahnel, J. Phys. Chem. 221 (2007) 349–360.
[42] D. Naumann, C. Schultz, A. Sabich, M. Kasrowsky, H. Labishinsi, J. Mol. Struct. 214 (1989) 213–246.
[43] J. Kiwi, V. Nadtochenko, J. Phys. Chem. B 108 (2004) 17675–17684.